

Space-Time Medium Functions as a Perfect Antenna-Mixer-Amplifier Transceiver

Sajjad Taravati and George V. Eleftheriades

*The Edward S. Rogers Sr. Department of Electrical and Computer Engineering,
University of Toronto, Toronto,
Ontario M5S 3H7, Canada
Email: sajjad.taravati@utoronto.ca*

We show that a space-time-varying medium can function as a front-end transceiver, i.e., an antenna-mixer-amplifier. Such a unique functionality is endowed by space-time surface waves associated with complex space-time wave vectors in a subluminal space-time medium. The proposed structure introduces pure frequency up- and down-conversions and with very weak undesired time harmonics. In contrast to other recently proposed space-time mixers, a large frequency up-/down conversion ratio, associated with gain is achievable. Furthermore, as the structure does not operate based on progressive energy transition between the space-time modulation and the incident wave, it possesses a subwavelength thickness (metasurface). Such a multi-functional, highly efficient and compact medium is expected to find various applications in modern wireless telecommunication systems.

I. INTRODUCTION

Reception and transmission of electromagnetic waves is the essence of wireless telecommunications [1, 2]. Such a task requires various functions, such as power amplification, frequency conversion, and wave radiation. These functions have been conventionally performed by electronic components and electromagnetic structures, such as transistor-based amplifiers, semiconductor-based diode mixers, and resonance-based antennas. The ever increasing demand for versatile wireless telecommunication systems has led to a substantial need in multi-functional components and compact integrated circuits. In general, each natural medium may introduce a single function, e.g., a resonator may operate as an antenna at a specific frequency. To contrast this conventional approach, a single medium exhibiting several functions concurrently could lead to a disruptive evolution in telecommunication technology.

Recently, space-time-modulated media have attracted a surge of scientific interest thanks to their capability in multifunctional operations, e.g., mixer-duplexer-antenna [3], unidirectional beam splitters [4], nonreciprocal filters [5, 6], and signal coding metagratings [7]. In addition, a large number of versatile and high efficiency electromagnetic systems have been recently reported based on the unique properties of space-time modulation, including space-time metasurfaces for advanced wave engineering and extraordinary control over electromagnetic waves [8–25], nonreciprocal platforms [26–32], frequency converters [17, 33], and time-modulated antennas [34–39]. Such strong capability of space-time-modulated media is due to their unique interactions with the incident field [21, 28, 40–44].

This paper reveals that a space-time medium can function as a full transceiver front-end, that is, an antenna-mixer-amplifier-filter system. Specific related contributions of this study are as follows.

- We show that the space-time medium operates as

an antenna per se. Such an interesting functionality of the space-time medium is endowed by space-time surface waves. Other recently proposed space-time antenna systems are formed by integration of the space-time-modulated medium with an antenna [3, 35, 45], and hence suffer from a number of drawbacks, i.e., requiring long structures, low efficiency and narrow-band operation.

- The proposed antenna-mixer-amplifier introduces large frequency up- and -down conversion ratios. This is very practical, because in real-scenario wireless telecommunication systems, a large frequency conversion is required, i.e., a frequency conversion from a microwave/millimeter-wave frequency to an intermediate frequency in receivers. In contrast, recently proposed space-time frequency converters suffer from very low frequency conversion ratios (up-/down-converted frequency is very closed to the input frequency) [3, 17, 35, 45].
- Recently proposed space-time systems operate based on a progressive coupling between the incident wave and the space-time modulation [3, 33, 46–48], and hence a thick (compared to the wavelength) slab is required. In contrast, the proposed antenna-mixer-amplifier does not work based on progressive coupling between the incident wave and the space-time modulation and hence is formed by a thin (sub-wavelength) slab. As a result, the proposed structure is classified among metasurface categories and is compatible with the compactness requirements of modern wireless telecommunication systems.
- The proposed medium inherently operates as a band-pass filter, i.e., a pure frequency down- and up-conversions occurs so that the undesired time harmonics are highly suppressed. Such a property is governed by the subluminal operation of space-time modulation.

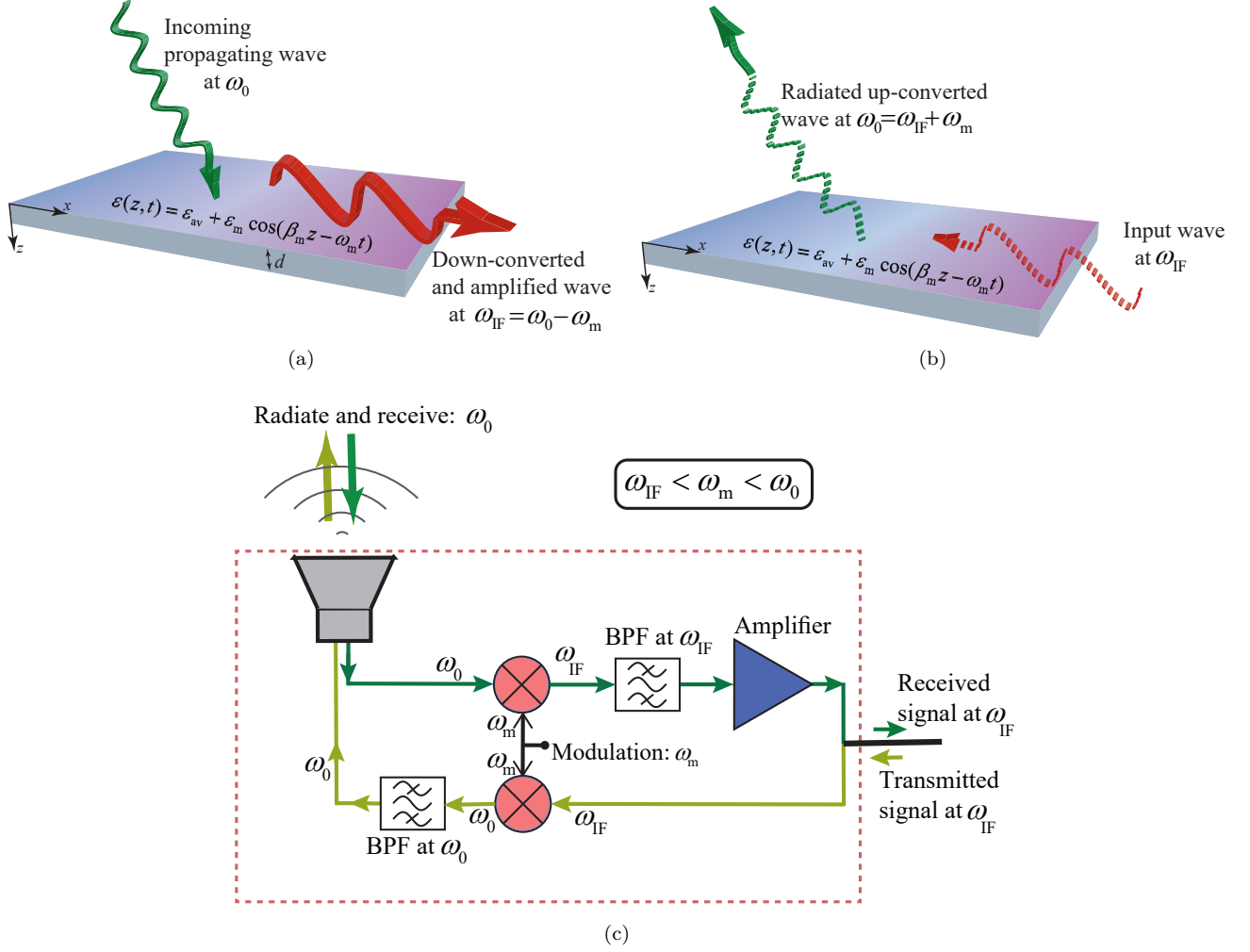


FIG. 1. Functionality of the antenna-mixer-amplifier space-time surface wave medium. (a) Down-link (reception) state, where a strong transition between a space-wave at ω_0 to a space-time surface wave at $\omega_{IF} = \omega_0 - \omega_m$ occurs. (b) Up-link (transmission) state, where a transition between a space-time surface wave at ω_{IF} to a space-wave at $\omega_0 = \omega_{IF} + \omega_m$ occurs. (c) Circuitual representation of the combined antenna-mixer-amplifier space-wave medium in (a) and (b).

- In contrast to conventional mixers that introduce a significant conversion loss, here a conversion gain may be achieved in the down-link or up-link. In addition, the radiation from the antenna-mixer-amplifier is very directive.

The paper is organized as follows. Section II presents the operation principle of the antenna-mixer-amplifier. Then, Sec. III investigates the theoretical aspects of the work, and provides an analysis of the wave propagation in the antenna-mixer-amplifier space-time medium. Next, Sec. IV presents the design procedure of the structure, and gives an approximate closed-form solution to calculate the thickness and receive/transmit power gain of the structure. Section V gives the time and frequency domain numerical simulation results for the designed antenna-mixer-amplifier. Finally, Sec. VI concludes the paper.

II. OPERATION PRINCIPLE

Consider the antenna-mixer-amplifier slab in Fig. 1(a), with the thickness of d and a spatiotemporally-periodic electric permittivity as

$$\epsilon(z, t) = \epsilon_{av} + \epsilon_m \cos(\beta_m z - \omega_m t), \quad (1)$$

with ϵ_{av} being the average electric permittivity of the background medium, and ϵ_m representing the modulation amplitude. In Eq. (1), ω_m denotes the temporal frequency of the modulation, and β_m is the spatial frequency of the modulation represented by

$$\beta_m = \frac{\omega_m}{v_m} = \frac{\omega_m}{\Gamma v_b}, \quad (2)$$

where v_m and v_b are the phase velocity of the modulation and the background medium, respectively, and $\Gamma = v_m/v_b$ is the space-time velocity ratio [28].

The slab in Fig. 1(a) is obliquely illuminated by a y -polarized incident electric field under an angle of incidence of θ_i , as

$$\mathbf{E}_i(x, z, t) = \hat{\mathbf{y}} E_i e^{i(k_x x + k_z z - \omega_0 t)}, \quad (3)$$

where E_i is the amplitude of the incident wave, and ω_0 and $k_0 = \sqrt{k_x^2 + k_z^2} = \sqrt{(k_0 \sin(\theta_i))^2 + (k_0 \cos(\theta_i))^2}$ are respectively temporal and spatial frequencies of the incident wave. Here, $k_0 = \omega_0/c$, with c being the velocity of light in vacuum.

In the receiving state (down-link) in Fig. 1(a), strong transition between a space-wave, with temporal frequency ω_0 , to a space-time surface wave, with temporal frequency $\omega_{\text{IF}} = \omega_0 - \omega_m$, occurs. In the transmission state (up-link) in Fig. 1(b) a transition between a space-time surface wave at ω_{IF} to a space-wave at $\omega_0 = \omega_{\text{IF}} + \omega_m$ occurs.

Figure 1(c) shows an equivalent circuit representation of the antenna-mixer-amplifier in Figs. 1(a) and 1(b). Thanks to the unique properties of space-time-modulated media, that will be described later in this study, such a medium introduces the functionality of a highly directive antenna, a pure frequency up-converter, a pure frequency down-converter, up-link and down-link filters, and a down-link amplifier. Such a rich functionality has not been experienced in other media unless several components and media are integrated, as shown in Fig. 1(c). However, here we show that a single medium can offer such versatile and useful operation.

As the slab is periodic in both space and time, the spatial and temporal frequencies of the space-time harmonics inside the structure are governed by the momentum conservation law, i.e.,

$$\gamma_{z,n} = \beta_{z,0} + n\beta_m + i\alpha_{z,n}, \quad (4a)$$

and the energy conservation law, i.e.,

$$\omega_n = \omega_0 + n\omega_m. \quad (4b)$$

The scattering angles of the space-time harmonics in regions 1 and 3 (reflection to the top and transmission to the bottom of the medium, respectively) may be determined by the Helmholtz relations, i.e., $k_0^2 \sin^2(\theta_i) + k_{0,n}^2 \cos^2(\theta_{rn}) = k_{0,n}^2$ and $k_0^2 \sin^2(\theta_i) + k_{0,n}^2 \cos^2(\theta_{tn}) = k_{0,n}^2$, with θ_{rn} and θ_{tn} being the reflection and transmission angles of the n^{th} space-time harmonics, reading [7]

$$\theta_{rn} = \theta_{tn} = \sin^{-1} \left(\frac{\sin(\theta_i)}{1 + n\omega_m/\omega_0} \right), \quad (5)$$

where $k_{0n} = \omega_n/c = (\omega_0 + n\omega_m)/c$. Therefore, given the common tangential wavenumber, $k_x = k_0 \sin(\theta_i)$ in all the regions, the reflection and transmission angles for the n^{th} space-time harmonic are equal. Equation (5) shows that the harmonics in the n -interval $[\omega_0(\sin \theta_i - 1)/\omega_m, +\infty]$ are scattered at different angles ranging from 0 to $\pi/2$ through θ_i for $n = 0$. However, the space-time

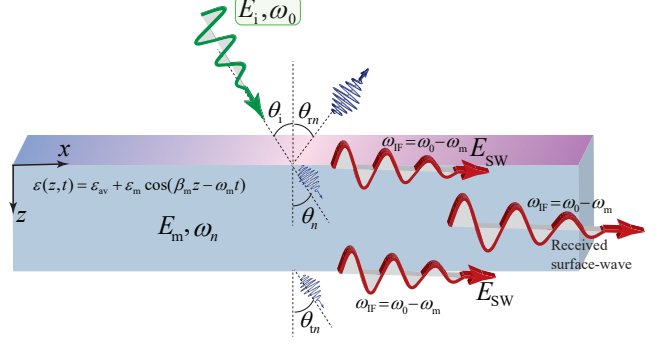


FIG. 2. Operation principle of the antenna-mixer-amplifier space-time medium. Transition of the incident space-wave to space-time surface waves at the two boundaries of the medium ($\theta_{r,-1} = \theta_{t,-1} = 90^\circ$) as well as inside it ($\theta_{-1} = 90^\circ$).

harmonics outside of this interval represent imaginary $k_{z,n}$ and hence propagate as space-time surface waves along the two boundaries of the slab at $z = 0$ and $z = d$.

The scattering angles of the space-time harmonics inside the space-time-modulated medium read

$$\theta_n = \tan^{-1} \left(\frac{k_x}{\beta_{z,n}} \right) = \tan^{-1} \left(\frac{k_0 \sin(\theta_i)}{\beta_{z,0} + n\beta_m} \right). \quad (6)$$

Figure 2 shows the structure of the antenna-mixer-amplifier space-time medium. We aim to design the structure such that the first lower space-time harmonic, $n = -1$, outside the medium scatters along the boundary of the medium, i.e., $\theta_{r,-1} = \theta_{t,-1} = 90^\circ$. Hence, using Eq. (5), the incident angle reads

$$\theta_i = \sin^{-1} \left(1 - \frac{\omega_m}{\omega_0} \right). \quad (7)$$

In addition, to achieving a strong transition to the $n = -1$ harmonic, the scattered $n = -1$ harmonic inside the medium should propagate in parallel to the two space-time surface waves on the two boundaries of the medium at $z = 0$ and $z = d$, i.e., $\theta_{n=-1} = 90^\circ$. Thus, using Eq. (6), we achieve

$$\beta_{z,-1} = 0. \quad (8)$$

As a result, the z component of the Wave vector inside the medium is purely imaginary, i.e., $\gamma_{z,-1} = i\alpha_{z,-1}$, whereas the incident field wavenumber k_z is purely real.

The space-time-modulated medium presents transition from the fundamental harmonic $n = 0$ to a large (theoretically infinite, $-\infty < n < \infty$) number of space-time harmonics. Such a transition is very strong for the luminal space-time modulation, where the space-time modulation velocity is close to the background phase velocity, i.e., $v_m = v_b$ [28, 30].

To prevent generation of strong undesired time harmonics, here the space-time-modulated medium operates

in the subluminal regime, where $0 < v_m < v_b$, i.e.,

$$0 < \Gamma_{\text{subluminal}} < \sqrt{\frac{\epsilon_r}{\epsilon_{\text{av}} + \epsilon_m}}. \quad (9)$$

As a result, a pure and precise transition between the fundamental ($n = 0$) harmonic and the desired (here $n = -1$) space-time surface wave harmonic can occur.

III. THEORETICAL INVESTIGATION

A. Analytical solution

Considering the TE_y incident field in Eq. (3), the incident magnetic field reads

$$\begin{aligned} \mathbf{H}_i(x, z, t) &= \frac{1}{\eta_1} [\hat{\mathbf{k}}_i \times \mathbf{E}_i^F(x, z, t)] \\ &= [-\hat{\mathbf{x}} \cos(\theta_i) + \hat{\mathbf{z}} \sin(\theta_i)] \frac{E_0}{\eta_1} e^{i(k_x x + k_z z - \omega_0 t)}, \end{aligned} \quad (10)$$

where $\eta_1 = \sqrt{\mu_0/\epsilon_0}$ is the characteristic impedance of free space. Since the space-time-modulated medium is periodic in space and time, the electric and magnetic fields in the slab may be decomposed to space-time Bloch-Floquet harmonics, as

$$\mathbf{E}_m(x, z, t) = \hat{\mathbf{y}} \sum_n \mathbf{E}_n e^{i\gamma_{z,n} z} e^{i(k_x x - \omega_n t)}, \quad (11a)$$

and

$$\mathbf{H}_m(x, z, t) = \frac{1}{k} \sum_n \mathbf{H}_n [-\hat{\mathbf{x}} \beta_{z,n} + \hat{\mathbf{z}} k_x] e^{i\gamma_{z,n} z} e^{i(k_x x - \omega_n t)}. \quad (11b)$$

The unknown coefficients in Eqs. (11a) and (11b), $\gamma_{z,n} = \beta_{z,n} + i\alpha_{z,n}$, E_n and H_n shall be found through the following procedure. We first construct and solve the corresponding wave equation. Next, we fix the source frequency ω_0 and then find the corresponding discrete $\gamma_{z,n}$ solutions, which form the dispersion diagram of the space-time medium. We next apply the spatial boundary conditions at the edges of the slab, i.e. at $z = 0$ and $z = d$, for all the $(\omega_0, \gamma_{z,n})$ states in the dispersion diagram. This provides the unknown field coefficients E_n and H_n inside the slab, as well as the scattered (reflected and transmitted) fields outside the slab, i.e., E_R and E_T .

The homogeneous wave equation reads

$$\nabla^2 \mathbf{E}_m(x, z, t) - \frac{1}{c^2} \frac{\partial^2 [\epsilon(z, t) \mathbf{E}_m(x, z, t)]}{\partial t^2} = 0. \quad (12)$$

Inserting (11a) and (1) into (12), and using the Fourier series expansion for the permittivity, results in

$$E_n \left[\frac{k_x^2 + (\beta_{z,n} + i\alpha_{z,n})^2}{[(\omega_0 + n\omega_m)/c]^2} \right] - \sum_{k=-\infty}^{\infty} \tilde{\epsilon}_k E_{n-k} = 0. \quad (13)$$

where $\tilde{\epsilon}_k$ are the Fourier series coefficients of the permittivity. Equation (13) may be cast to the matrix form as

$$[K] \cdot [E_n] = 0, \quad (14)$$

where $[K]$ is the $(2N+1) \times (2N+1)$ matrix with elements

$$\begin{aligned} K_{nn} &= \left[\frac{k_x^2 + (\beta_{z,n} + i\alpha_{z,n})^2}{[(\omega_0 + n\omega_m)/c]^2} \right] - \epsilon_0, \\ K_{nk} &= -\tilde{\epsilon}_{n-k}, \quad \text{for } n \neq k, \end{aligned} \quad (15)$$

where $2N+1$ is the number of truncated harmonics. Then, the dispersion relation reads

$$\det \{[K]\} = 0, \quad (16)$$

Once the dispersion diagram is formed, for a given incident temporal frequency ω_0 , the corresponding wave number, i.e., $\gamma_{z,n}$, inside the slab can be computed. Next, the unknown field amplitudes E_n in the slab are found by solving (14) after determining the E_0 satisfying boundary conditions. Figure 3 shows a qualitative 3D dispersion diagram of a subluminal space-time modulated medium, composed of an infinite periodic set of double-cones with apexes at $\beta_{z,0} = -n\beta_m$ and $k_x = 0$ and the slope Γ . As the slope Γ increases and goes towards unity, the cones get closer to each other and start touching other cones (harmonics). As a result, stronger transition between harmonics occurs and yields transitions of the power from the fundamental harmonic to a large number of harmonics. However, this is not what we aim at. As we are interested in a pure transition to a desired harmonic ($n = -1$), we require a subluminal space-time modulation defined in Eq. (9).

Figure 4 plots the analytical isofrequency dispersion diagram, computed using (16), for the subluminal regime where $\Gamma = 0.2$. We have chosen a specific θ_i , where the $n = -1$ harmonic is excited at a point corresponding to $\beta_{z,-1} = 0$ (i.e., $\beta_{z,0}/\beta_m = +1$). As a consequence, the $n = -1$ harmonic scatters along the x -direction, i.e., $\theta_{r,-1} = 90^\circ$. Although the real part of the z component of the wavevector of the $n = -1$ harmonic is zero ($\beta_{z,-1} = 0$), its imaginary part is greater than zero, and hence $\gamma_{z,-1} = i\alpha_{z,-1}$.

Figure 4 shows that the transition between the forward $n = 0$ and $n = -1$ harmonics (highlighted with magenta arrows) occurs for both reception (down-link) and transmission (up-link). This may as well be verified by Eq. (6) as follows. For the down-link, the incident wave ($n = 0$) with the incident angle of θ_i^{RX} and wavenumber of $\beta_{z,0}^{\text{RX}} = \beta_m$ makes a transition to the down-converted harmonic ($n = -1$), which is attributed to $\theta_{-1}^{\text{RX}} = 90^\circ$, $\beta_{z,-1}^{\text{RX}} = 0$ and $\gamma_{z,-1}^{\text{RX}} = i\alpha_{z,-1}^{\text{RX}}$. However, for the up-link (transmission state), the incident wave ($n = 0$) with the incident angle of $\theta_i^{\text{TX}} = 90^\circ$ and wavenumber of $\beta_{z,0}^{\text{TX}} = 0$ makes a transition to the up-converted harmonic ($n = +1$) with $\theta_{+1}^{\text{TX}} = \theta_0^{\text{RX}} = \theta_i^{\text{RX}}$, which is attributed to $\beta_{z,+1}^{\text{TX}} = \beta_m$ and $\gamma_{z,+1}^{\text{TX}} = \beta_m$.

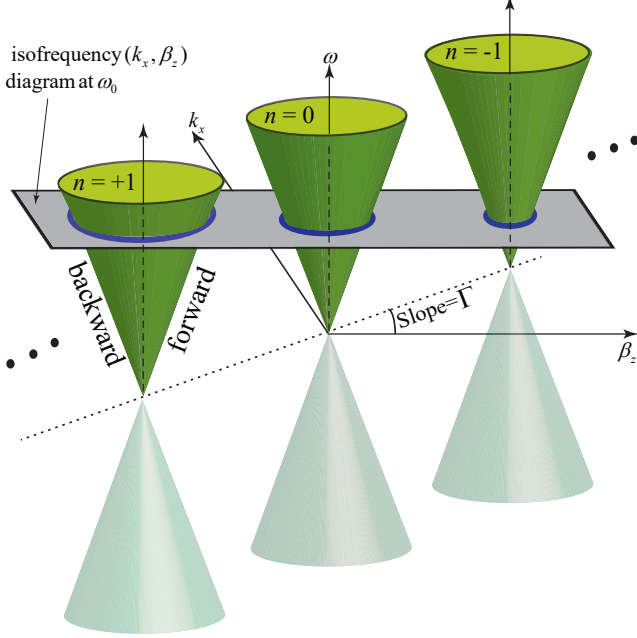


FIG. 3. 3D-dispersion diagram of the space-time medium, formed by an infinite number of double cones each of which representing a space-time harmonic.

IV. DESIGN PROCEDURE

A. Complex Dispersion Diagrams

Figure 5(a) plots the analytical isofrequency dispersion diagram $(\beta_{z,n}(k_x))$ at $\omega/\omega_m = 1.363$ of the sinusoidally space-time surface wave medium with the electric permittivity in (1) for the subluminal regime, i.e., $\Gamma = 0.55$ for $\epsilon_m \rightarrow 0$. It may be seen from this figure that forward $n = 0$ and $n = -1$ harmonics are excited very close to each other, where $n = 0$ is excited at an angle of scattering of $\theta_0 = \theta_i = 15^\circ$. However, the $n = -1$ harmonic is intentionally excited at the angle of scattering of $\theta_{-1} = 90^\circ$.

Figure 5(b) plots the same isofrequency $\beta_{z,n}(k_x)$ diagram as Figure 5(a) except for a greater modulation amplitude of $\epsilon_m = 0.45$. As a result of non-equilibrium in the electric and magnetic permittivities of the medium, several electromagnetic badgaps appear at the intersections between space-time harmonics [30]. As a consequence, strong coupling between some of the harmonics has occurred, e.g. between the $n = 0$ and $n = -1$ harmonics.

Figure 5(c) plots the complex isofrequency dispersion diagram $\gamma_{z,n}(k_x)$ for the medium in Fig. 5(b). This diagram is formed by two different curves, i.e., the real $\beta_{z,n}(k_x)$ and the imaginary $\alpha_{z,n}(k_x)$ parts of the wavenumber. For the sake of clarification, we have included only a few number of harmonics. This figure shows that at the excited angle of incidence $\theta_i = 15^\circ$, the $n = 0$ harmonic introduces a pure real wavenumber, i.e., $\gamma_{z,0} = \beta_{z,0}$, whereas the $n = -1$ harmonic acquires

a pure imaginary wavenumber, that is, $\gamma_{z,-1} = i\alpha_{z,-1}$. As a result, a perfect space-time transition from a pure propagating wave to a pure space-time surface wave is ensured.

Figure 5(d) plots the complex dispersion diagram, i.e., $\gamma_{z,n}(\omega_0)$ for the medium in Fig. 5(b) and 5(c). This figure shows the strong transition between $n = 0$ and $n = -1$ harmonics from the $k_x = 0.218$ (corresponding to $\theta_i = 15^\circ$) cut.

B. Approximate closed-form solution

To best investigate the efficiency of the antenna-mixer-amplifier, we present an approximate closed-form solution. Such an approximate closed-form solution clearly shows the effect of modulation parameters on the efficiency of the proposed antenna-mixer-amplifier medium.

1. Reception state (down-link)

Equations (S7) and (S9) in the supplemental material form a matrix differential equation. For the down-link, the initial conditions of $E_0(0) = E_i$ and $E_{-1}(0) = 0$ gives

$$E_0(z) = E_i \cos\left(\frac{\epsilon_m k_0 k_{-1}}{4\sqrt{\gamma_{z,-1}\gamma_{z,0}}}z\right), \quad (17)$$

$$E_{-1}(z) = iE_i \frac{k_{-1}}{k_0} \sqrt{\frac{\gamma_{z,0}}{\gamma_{z,-1}}} \sin\left(\frac{\epsilon_m k_0 k_{-1}}{4\sqrt{\gamma_{z,-1}\gamma_{z,0}}}z\right), \quad (18)$$

where $k_{-1} = \omega_{-1}/c^2$. The optimal transition from the incident field to the space-time surface wave occurs at $z = d$, where

$$\frac{d}{dz}E_{-1}(z)|_{z=d} = 0, \quad (19)$$

yielding $|\epsilon_m k_0 k_{-1} d / (4\sqrt{\gamma_{z,-1}\gamma_{z,0}})| = \pi/2$ which corresponds to

$$d = 2\pi \left| \frac{\sqrt{\gamma_{z,-1}\gamma_{z,0}}}{\epsilon_m k_0 k_{-1}} \right|. \quad (20)$$

The down-link transition power ratio reads

$$G_d = \frac{|E_{-1}(z=d)|^2}{|E_i|^2} = \frac{|k_{-1}^2 \gamma_{z,0}|}{|k_0^2 \gamma_{z,-1}|} = \frac{\omega_{-1}^2 \beta_m}{\omega_0^2 \alpha_{z,-1}}, \quad (21)$$

Therefore, for a set of modulation parameters, i.e., ω_m , $\alpha_{z,-1}$ and Γ , a down-link power gain may be achieved. For the particular case, with the dispersion diagram in Figs. 5(c) and 5(d), since $\alpha_{z,-1} \ll \beta_m$ (i.e., $\alpha_{z,-1}/\beta_m = 0.03$ and $\omega_{-1}^2/\omega_0^2 = 0.071$), the down-link power gain reads $G_d = 3.75$ dB. This power gain emerges from the coupling of the space-time modulation power to the incident wave [4, 40, 49, 50].

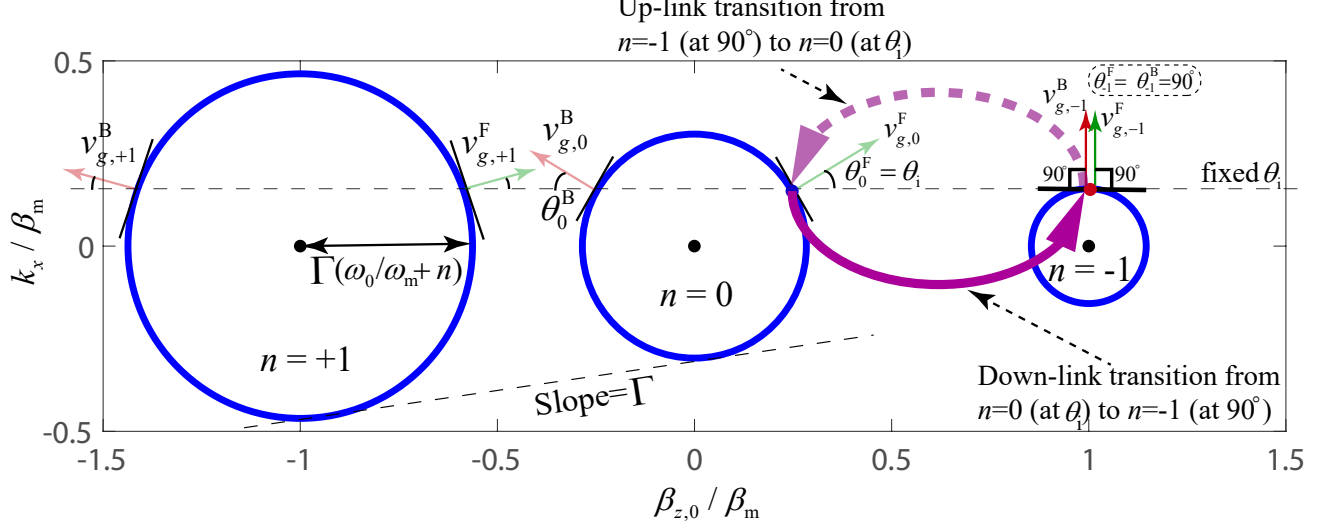


FIG. 4. Analytical isofrequency dispersion diagram for $\Gamma = 0.2$ and $\epsilon_m \rightarrow 0$, showing down-link (reception) and up-link (transmission) electromagnetic transitions between the fundamental propagating harmonic ($n = 0$) and the space-time surface wave harmonic ($n = -1$). Excitation of the medium at θ_i leads to excitation of the $n = -1$ at 90° .

The total down-link electric field inside the slab reads

$$E(x, z, t) = E_i \cos \left(\frac{\epsilon_m k_0 k_{-1}}{4\sqrt{i\alpha_{z,-1}\beta_{z,0}}} z \right) e^{-i(k_x x + \beta_{z,0} z - \omega_0 t)} + iE_i \frac{k_{-1}}{k_0} \sqrt{\frac{\beta_{z,0}}{i\alpha_{z,-1}}} \sin \left(\frac{\epsilon_m k_0 k_{-1}}{4\sqrt{i\alpha_{z,-1}\beta_{z,0}}} z \right) e^{-i(k_x x + i\alpha_{z,-1} z - \omega_{-1} t)}, \quad (22)$$

total up-link electric field inside the slab reads

$$E(x, z, t) = iE_i \frac{k_0}{k_{-1}} \sqrt{\frac{i\alpha_{z,-1}}{\beta_{z,0}}} \sin \left(\frac{\epsilon_m k_0 k_{-1}}{4\sqrt{i\alpha_{z,-1}\beta_{z,0}}} z \right) e^{-i(k_x x + \beta_{z,0} z - \omega_0 t)} + E_i \cos \left(\frac{\epsilon_m k_0 k_{-1}}{4\sqrt{i\alpha_{z,-1}\beta_{z,0}}} z \right) e^{-i(k_x x + i\alpha_{z,-1} z - \omega_{-1} t)}. \quad (26)$$

2. Transmission state (up-link)

For the up-link, the matrix differential equations (S7) and (S9) with the initial conditions of $E_{-1}(0) = E_i$ and $E_0(0) = 0$ yields

$$E_{-1}(z) = E_i \cos \left(\frac{\epsilon_m k_0 k_{-1}}{4\sqrt{\gamma_{z,-1}\gamma_{z,0}}} z \right), \quad (23)$$

$$E_0(z) = iE_i \frac{k_0}{k_{-1}} \sqrt{\frac{\gamma_{z,-1}}{\gamma_{z,0}}} \sin \left(\frac{\epsilon_m k_0 k_{-1}}{4\sqrt{\gamma_{z,-1}\gamma_{z,0}}} z \right). \quad (24)$$

The up-link transition power ratio reads

$$G_u = \frac{|E_0(z=d)|^2}{|E_i|^2} = \left| \frac{k_0^2 \gamma_{z,-1}}{k_{-1}^2 \gamma_{z,0}} \right| = \frac{\omega_0^2 \alpha_{z,-1}}{\omega_{-1}^2 \beta_m}, \quad (25)$$

which is the inverse of the down-link transition power ratio. This shows that the proposed antenna-mixer-amplifier introduces a power amplification only in one direction (here down-link), as shown in Fig. 1(c). The

V. RESULTS

This section investigates the functionality and efficiency of the antenna-mixer-amplifier space-time slab using FDTD numerical simulation. We consider oblique incidence to the slab and compare the numerical results with the analytical solution provided in Secs. III A and IV B. Figure 6(a) depicts the structure of the antenna-mixer-amplifier space-time surface wave medium. A substrate integrated waveguide (SIW) is integrated with the space-time slab to efficiently launch and receive space-time surface waves. The slab assumes $\omega_m = 2\pi \times 2.2$ GHz, $\epsilon_m = 0.45$, $\Gamma = 0.55$, and $d = 0.8\lambda_0$. A plane wave with temporal frequency $\omega_0 = 2\pi \times 3$ GHz is propagating in the $+z$ -direction under an angle of incidence of $\theta_i = 15^\circ$, and impinges on the slab.

Figure 6(b) shows the time domain numerical simulation result for the receiving state (down-link). It may be seen from this figure that a pure transition from the incident space-wave at ω_0 to the space-time surface wave, propagating along the x -direction, at frequency $\omega_{IF} = \omega_0 - \omega_m = 2\pi \times 0.8$ GHz occurs. Furthermore, it may be seen from Fig. 6(b) that the amplitude of the

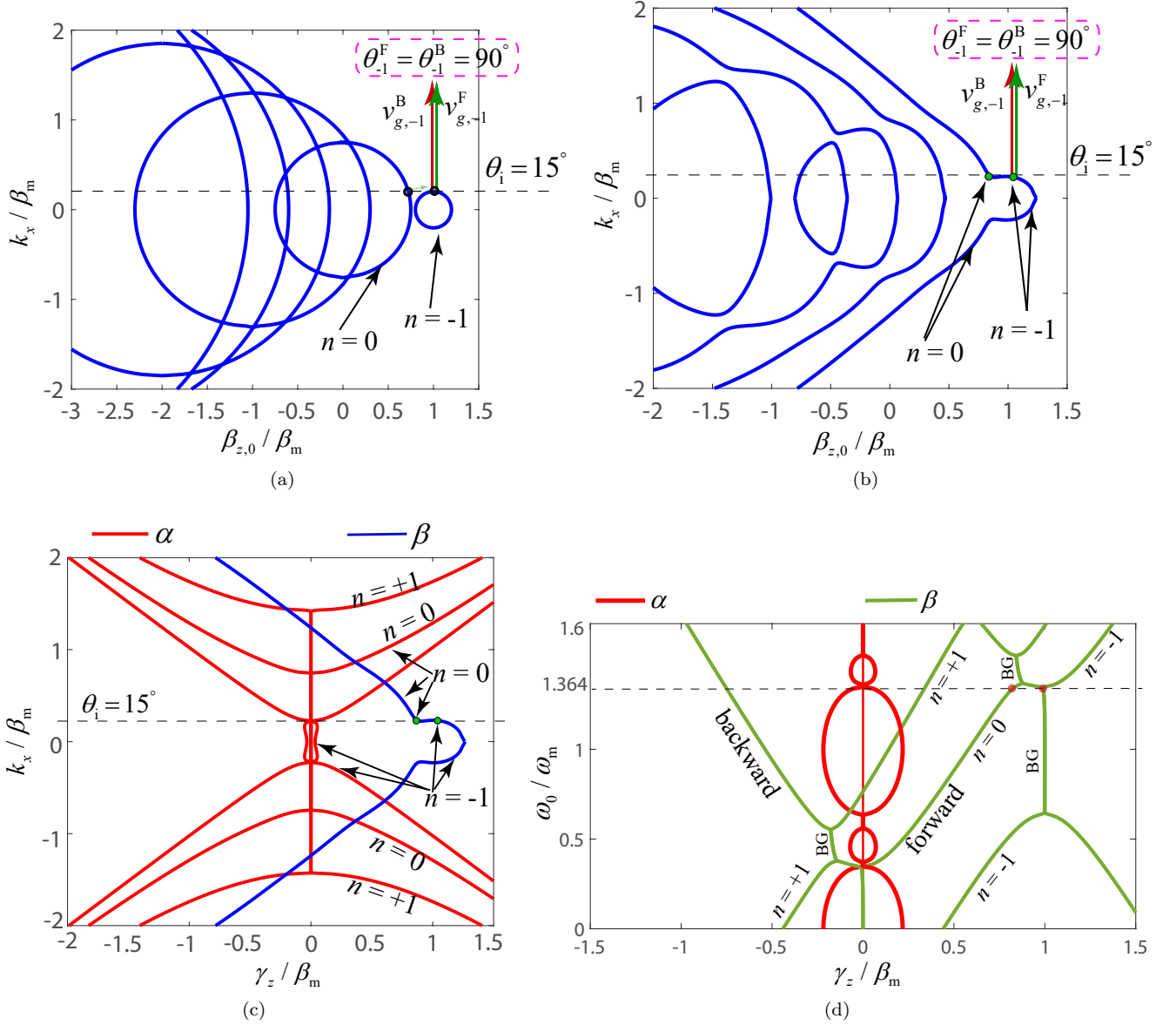


FIG. 5. Analytical dispersion diagram of the sinusoidally space-time surface wave medium with the electric permittivity in (1) for subluminal regime, i.e., $\Gamma = 0.55$. (a) Isofrequency diagram, i.e., $\beta_{z,n}(k_x)$ at $\omega/\omega_m = 1.363$, and for $\epsilon_m \rightarrow 0$. (b) Same as (a) except for greater modulation amplitude $\epsilon_m = 0.45$. (c) Isofrequency diagram of the medium in (b), which includes the real and imaginary parts of the $\gamma_{z,n}$, i.e., $\beta_{z,n}$ and $\alpha_{z,n}$, for $n = 0$ and $n = -1$. (d) Dispersion diagram, i.e., $\gamma_{z,n}(\omega_0)$ for the medium in (a) and (b) for the $k_x = 0.218$ (corresponding to $\theta_i = 15^\circ$) cut.

received wave is stronger than the amplitude of the incident wave. Figure 6(c) plots the frequency domain numerical simulation result. This plot clearly shows a pure and strong transition (frequency-conversion) from the incident wave to the down-converted space-time surface wave. The 3.5 dB power conversion gain is in agreement with the analytical result in Eq. (21). In addition, the amplitudes of the undesired harmonics are more than 33 dB lower than the amplitude of the down-converted harmonic at ω_{IF} .

Figure 7(a) shows the time domain FDTD numeri-

cal simulation result for the transmission state (up-link). Here, a transition (up-conversion) from the space-time surface wave at ω_{IF} to the space-wave at $\omega_0 = \omega_{IF} + \omega_m$ occurs.

Figure 7(b) plots the frequency domain numerical simulation result for the transmission state (up-link). This plot clearly shows a pure and strong transition (frequency-conversion) from the incident wave to the down-converted space-time surface wave. The 3.52 dB power conversion loss is in agreement with the analytical result in Eq. (25). In addition, the amplitude of the un-

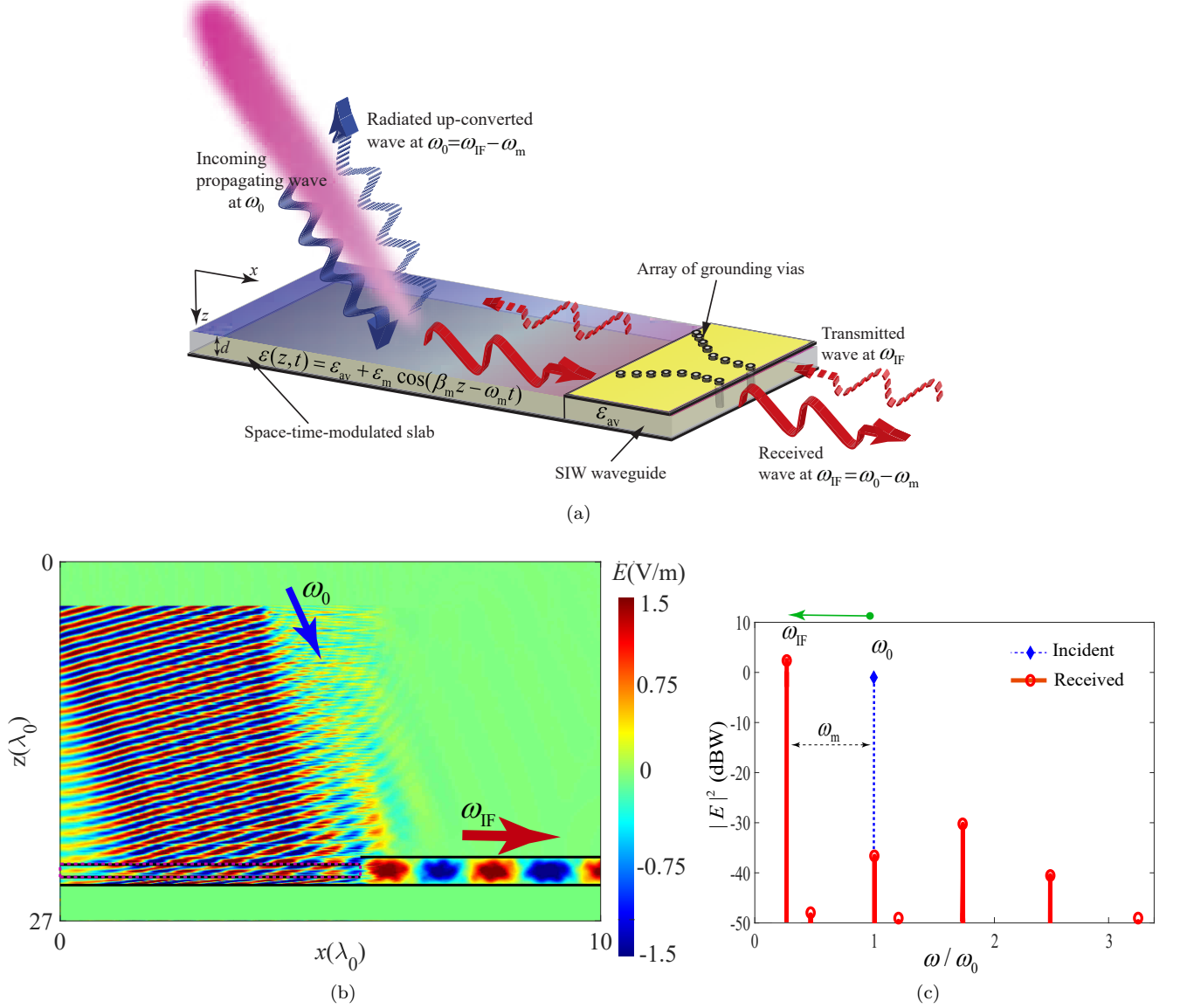


FIG. 6. FDTD simulation results of the antenna-mixer-amplifier space-time surface wave medium with $\omega_0/\omega_m = 1.363$, $\epsilon_m = 0.45$, $d = 0.8\lambda_0$, and $\theta_i = 15^\circ$. (a) Architecture of the medium. (b) Time- and (c) frequency-domain responses for the down-link transition.

desired harmonics are more than 27 dB lower than the amplitude of the down-converted harmonic at ω_0 .

VI. CONCLUSIONS

We showed that a space-time-varying medium operates as an antenna-mixer-amplifier. Such a unique functionality is achieved by taking advantages of space-time surface waves associated with complex space-time wave vectors in a subluminal space-time medium. The proposed structure is endowed with pure frequency up- and down-conversions and very weak undesired time harmon-

ics. In contrast to the recently proposed space-time mixers, a large frequency ratio between the incident wave frequency and the up-/down-converted wave frequency, with a down- or up-conversion gain, is achievable. Furthermore, as the structure does not operate based on progressive energy transition between the space-time modulation and the incident wave, it possesses a subwavelength thickness (metasurface). Such a multi-functional, highly efficient and compact medium represents a new class of integrated electronic-electromagnetic component, and is expected to find various applications in modern wireless telecommunication systems.

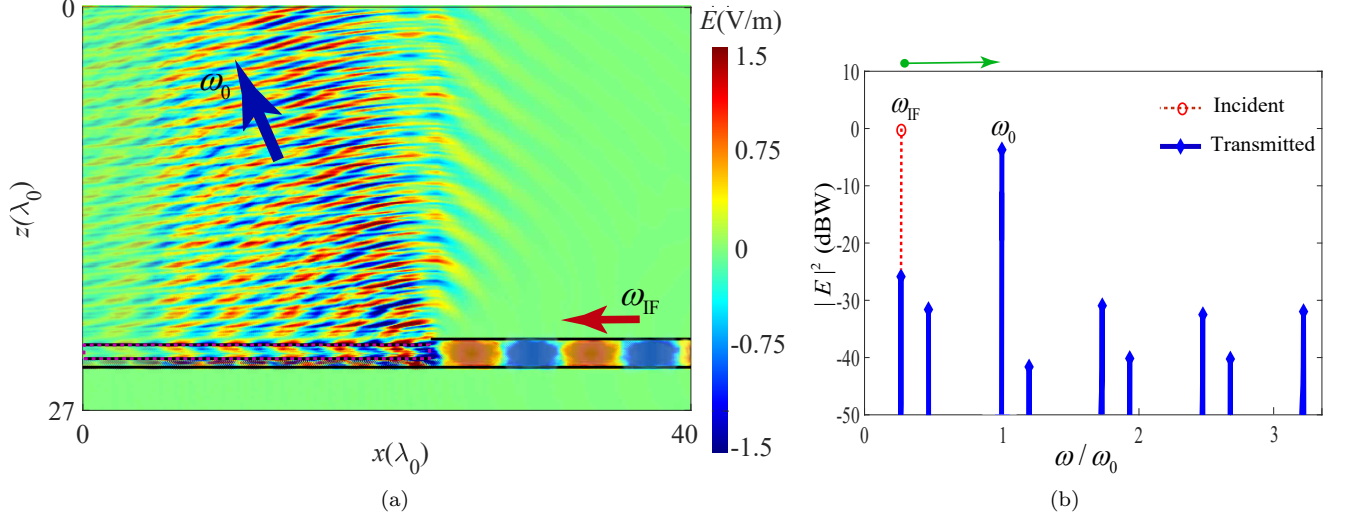


FIG. 7. FDTD simulation results of the antenna-mixer-amplifier space-time surface wave medium with $\omega_0/\omega_m = 1.363$, $\epsilon_m = 0.45$, $d = 0.8\lambda_0$, and $\theta_i = 15^\circ$. (a) and (b) Time-domain and frequency-domain responses for the up-link transition.

- [1] G. Vannucci, "Wireless telecommunication system," 1995, US Patent 5,459,727.
- [2] S. R. Saunders and A. Aragón-Zavala, *Antennas and propagation for wireless communication systems*. John Wiley & Sons, 2007.
- [3] S. Taravati and C. Caloz, "Mixer-duplexer-antenna leaky-wave system based on periodic space-time modulation," *IEEE Trans. Antennas Propagat.*, vol. 65, no. 2, pp. 442–452, Feb. 2017.
- [4] S. Taravati and A. A. Kishk, "Dynamic modulation yields one-way beam splitting," *Phys. Rev. B*, vol. 99, no. 7, p. 075101, Jan. 2019.
- [5] A. Alvarez-Melcon, X. Wu, J. Zang, X. Liu, and J. S. Gomez-Diaz, "Coupling matrix representation of non-reciprocal filters based on time-modulated resonators," *IEEE Trans. Microw. Theory Techn.*, vol. 67, no. 12, pp. 4751–4763, 2019.
- [6] X. Wu, X. Liu, M. D. Hickle, D. Peroulis, J. S. Gómez-Díaz, and A. Á. Melcón, "Isolating bandpass filters using time-modulated resonators," *IEEE Trans. Microw. Theory Techn.*, vol. 67, no. 6, pp. 2331–2345, 2019.
- [7] S. Taravati and G. V. Eleftheriades, "Generalized space-time periodic diffraction gratings: Theory and applications," *Phys. Rev. Appl.*, vol. 12, no. 2, p. 024026, 2019.
- [8] Y. Shi and S. Fan, "Dynamic non-reciprocal metasurfaces with arbitrary phase reconfigurability based on photonic transition in meta-atoms," *Appl. Phys. Lett.*, vol. 108, p. 021110, Jan. 2016.
- [9] Y. Shi, S. Han, and S. Fan, "Optical circulation and isolation based on indirect photonic transitions of guided resonance modes," *ACS Photonics*, vol. 4, no. 7, pp. 1639–1645, Jun. 2017.
- [10] M. M. Salary, S. Jafar-Zanjani, and H. Mosallaei, "Electrically tunable harmonics in time-modulated metasurfaces for wavefront engineering," *New J. Phys.*, vol. 20, no. 12, p. 123023, 2018.
- [11] M. M. Salary, S. Farazi, and H. Mosallaei, "A dynamically modulated all-dielectric metasurface doublet for directional harmonic generation and manipulation in transmission," *Adv. Opt. Mater.*, p. 1900843, 2019.
- [12] S. Taravati and A. A. Kishk, "Advanced wave engineering via obliquely illuminated space-time-modulated slab," *IEEE Trans. Antennas Propagat.*, vol. 67, no. 1, pp. 270–281, 2019.
- [13] J. W. Zang, D. Correias-Serrano, J. T. S. Do, X. Liu, A. Alvarez-Melcon, and J. S. Gomez-Diaz, "Nonreciprocal wavefront engineering with time-modulated gradient metasurfaces," *Phys. Rev. Appl.*, vol. 11, no. 5, p. 054054, 2019.
- [14] S. Inampudi, M. M. Salary, S. Jafar-Zanjani, and H. Mosallaei, "Rigorous space-time coupled-wave analysis for patterned surfaces with temporal permittivity modulation," *Opt. Mater. Express*, vol. 9, no. 1, pp. 162–182, 2019.
- [15] S. Y. Elnaggar and G. N. Milford, "Generalized space-time periodic circuits for arbitrary structures," *arXiv preprint arXiv:1901.08698*, 2019.
- [16] N. Wang, Z.-Q. Zhang, and C. Chan, "Photonic floquet media with a complex time-periodic permittivity," *Phys. Rev. B*, vol. 98, no. 8, p. 085142, 2018.
- [17] Z. Wu and A. Grbic, "Serrodyne frequency translation using time-modulated metasurfaces," *IEEE Trans. Antennas Propagat.*, 2019.
- [18] S. Taravati and A. A. Kishk, "Space-time modulation: Principles and applications," *IEEE Microw. Mag.*, vol. 21, no. 4, pp. 30–56, 2020.
- [19] G. A. Ptitcyn, M. S. Mirmoosa, and S. A. Tretyakov, "Time-modulated meta-atoms," *Phys. Rev. Res.*, vol. 1, no. 2, p. 023014, 2019.
- [20] H. B. Sedeh, M. M. Salary, and H. Mosallaei, "Topological space-time photonic transitions in angular-momentum-biased metasurfaces," *Advanced Optical Materials*.

- [21] Z.-X. Du, A. Li, X. Y. Zhang, and D. F. Sievenpiper, "A simulation technique for radiation properties of time-varying media based on frequency-domain solvers," *IEEE Access*, vol. 7, pp. 112 375–112 383, 2019.
- [22] X. Wang, A. Diaz-Rubio, H. Li, S. A. Tretyakov, and A. Alu, "Theory and design of multifunctional space-time metasurfaces," *Phys. Rev. Appl.*, vol. 13, no. 4, p. 044040, 2020.
- [23] S. Taravati and G. V. Eleftheriades, "Full-duplex nonreciprocal-beam-steering metasurfaces comprising time-modulated twin meta-atoms," *arXiv preprint arXiv:1911.04033*, 2019.
- [24] A. Li, Y. Li, J. Long, E. Forati, Z. Du, and D. Sievenpiper, "Time-modulated nonreciprocal metasurface absorber for surface waves," *Optics Letters*, vol. 45, no. 5, pp. 1212–1215, 2020.
- [25] H. B. Sedeh, M. M. Salary, and H. Mosallaei, "Topological space-time photonic transitions in angular-momentum-biased metasurfaces," *Adv. Opt. Mater.*, 2020.
- [26] S. Taravati, "Application of space-and time-modulated dispersion engineered metamaterials to signal processing and magnetless nonreciprocity," Ph.D. dissertation, École Polytechnique de Montréal, 2017.
- [27] J. L. Wentz, "A nonreciprocal electrooptic device," *Proc. IEEE*, vol. 54, no. 1, pp. 97–98, 1966.
- [28] S. Taravati, N. Chamanara, and C. Caloz, "Nonreciprocal electromagnetic scattering from a periodically space-time modulated slab and application to a quasisonic isolator," *Phys. Rev. B*, vol. 96, no. 16, p. 165144, Oct. 2017.
- [29] S. Taravati, "Self-biased broadband magnet-free linear isolator based on one-way space-time coherency," *Phys. Rev. B*, vol. 96, no. 23, p. 235150, Dec. 2017.
- [30] —, "Giant linear nonreciprocity, zero reflection, and zero band gap in equilibrated space-time-varying media," *Phys. Rev. Appl.*, vol. 9, no. 6, p. 064012, Jun. 2018.
- [31] M. Oudich, Y. Deng, M. Tao, and Y. Jing, "Space-time phononic crystals with anomalous topological edge states," *Phys. Rev. Res.*, vol. 1, no. 3, p. 033069, 2019.
- [32] M. Chegnizadeh, M. Memarian, and K. Mehrany, "Nonreciprocity using quadrature-phase time-varying slab resonators," *J. Opt. Soc. Am. B*, vol. 37, no. 1, pp. 88–97, 2020.
- [33] S. Taravati, "Aperiodic space-time modulation for pure frequency mixing," *Phys. Rev. B*, vol. 97, no. 11, p. 115131, 2018.
- [34] H. Shanks, "A new technique for electronic scanning," *IEEE Trans. Antennas Propag.*, vol. 9, no. 2, pp. 162–166, 1961.
- [35] Y. Hadad, J. C. Soric, and A. Alù, "Breaking temporal symmetries for emission and absorption," *Proc. Natl. Acad. Sci.*, vol. 113, no. 13, pp. 3471–3475, 2016.
- [36] D. Ramaccia, D. L. Sounas, A. Alù, F. Bilotti, and A. Toscano, "Nonreciprocity in antenna radiation induced by space-time varying metamaterial cloaks," *IEEE Antennas Wirel. Propagat. Lett.*, vol. 17, no. 11, pp. 1968–1972, 2018.
- [37] S. Taravati and A. A. Kishk, "Space-time-varying surface-wave antenna," in *2018 18th International Symposium on Antenna Technology and Applied Electromagnetics (ANTEM)*. IEEE, 2018.
- [38] M. M. Salary, S. Jafar-Zanjani, and H. Mosallaei, "Nonreciprocal optical links based on time-modulated nanoantenna arrays: Full-duplex communication," *Phys. Rev. B*, vol. 99, no. 4, p. 045416, 2019.
- [39] J. Zang, X. Wang, A. Alvarez-Melcon, and J. S. Gomez-Diaz, "Nonreciprocal yagi-uda filtering antennas," *IEEE Antennas Wirel. Propagat. Lett.*, vol. 18, no. 12, pp. 2661–2665, 2019.
- [40] J. Li, C. Shen, X. Zhu, Y. Xie, and S. A. Cummer, "Nonreciprocal sound propagation in space-time modulated media," *Phys. Rev. B*, vol. 99, no. 14, p. 144311, 2019.
- [41] D. C. Serrano, A. Alù, and J. S. Gomez-Diaz, "Magnetic-free nonreciprocal photonic platform based on time-modulated graphene capacitors," *Phys. Rev. B*, vol. 98, no. 16, p. 165428, 2018.
- [42] M. Liu, D. A. Powell, Y. Zarate, and I. V. Shadrivov, "Huygens metadevices for parametric waves," vol. 8, no. 3, p. 031077, 2018.
- [43] S. Y. Elnaggar and G. N. Milford, "Modelling space-time periodic structures with arbitrary unit cells using time periodic circuit theory," *arXiv preprint arXiv:1901.08698*, 2019.
- [44] S. Taravati and G. V. Eleftheriades, "Mixer-antenna medium," in *2019 13th International Congress on Artificial Materials for Novel Wave Phenomena (Metamaterials)*. IEEE, 2019.
- [45] S. Taravati and C. Caloz, "Space-time modulated nonreciprocal mixing, amplifying and scanning leaky-wave antenna system," in *IEEE AP-S Int. Antennas Propagat. (APS)*, Vancouver, Canada, 2015.
- [46] Z. Yu and S. Fan, "Complete optical isolation created by indirect interband photonic transitions," *Nat. Photonics*, vol. 3, pp. 91 – 94, Jan. 2009.
- [47] H. Lira, Z. Yu, S. Fan, and M. Lipson, "Electrically driven nonreciprocity induced by interband photonic transition on a silicon chip," *Phys. Rev. Lett.*, vol. 109, p. 033901, Jul. 2012.
- [48] N. Chamanara, S. Taravati, Z.-L. Deck-Léger, and C. Caloz, "Optical isolation based on space-time engineered asymmetric photonic bandgaps," *Phys. Rev. B*, vol. 96, no. 15, p. 155409, Oct. 2017.
- [49] A. L. Cullen, "A travelling-wave parametric amplifier," *Nature*, vol. 181, p. 332, Feb. 1958.
- [50] P. Tien and H. Suhl, "A traveling-wave ferromagnetic amplifier," *Proc. IEEE*, vol. 46, no. 4, pp. 700–706, 1958.

SUPPLEMENTAL MATERIAL

The antenna-mixer-amplifier space-time medium is placed between $z = 0$ and $z = d$, and represented by the space-time-varying permittivity of

$$\epsilon_{\text{eq}}(z, t) = \epsilon_{\text{av}} + \epsilon_{\text{m}} \cos(\beta_{\text{m}} z - \omega_{\text{m}} t), \quad (\text{S1})$$

and $\mu = \mu_0$. The electric field inside the slab is defined based on the superposition of the $m = 0$ and $m = -1$ space-time harmonics fields, i.e.,

$$E_{\text{S}}(x, z, t) = E_0(z) e^{-i(k_x x + \gamma_{z,0} z - \omega_0 t)} + E_{-1}(z) e^{-i(k_x x + \gamma_{z,-1} z - \omega_{-1} t)}, \quad (\text{S2})$$

where $\omega_{-1} = \omega_0 - \omega_{\text{m}}$. The corresponding homogeneous wave equation reads

$$\frac{\partial^2 \mathbf{E}}{\partial x^2} + \frac{\partial^2 \mathbf{E}}{\partial z^2} = \frac{1}{c^2} \frac{\partial^2 [\epsilon_{\text{eq}}(t, z) \mathbf{E}]}{\partial t^2}. \quad (\text{S3})$$

Inserting the electric field in (S2) into the wave equation in (S3) results in

$$\begin{aligned} & \left(\frac{\partial^2}{\partial x^2} + \frac{\partial^2}{\partial z^2} \right) \left[E_0(z) e^{-i(k_x x + \gamma_{z,0} z - \omega_0 t)} + E_{-1}(z) e^{-i(k_x x + \gamma_{z,-1} z - \omega_{-1} t)} \right] \\ &= \frac{1}{c^2} \frac{\partial^2}{\partial t^2} \left(\left[\epsilon_{\text{av}} + \frac{\epsilon_{\text{m}}}{2} e^{i(\beta_{\text{m}} z - \omega_{\text{m}} t)} + \frac{\epsilon_{\text{m}}}{2} e^{-i(\beta_{\text{m}} z - \omega_{\text{m}} t)} \right] \right. \\ & \quad \left. \times \left(E_0(z) e^{-i(k_x x + \gamma_{z,0} z - \omega_0 t)} + E_{-1}(z) e^{-i(k_x x + \gamma_{z,-1} z - \omega_{-1} t)} \right) \right), \end{aligned} \quad (\text{S4})$$

and applying the space and time derivatives, while using a slowly varying envelope approximation (i.e., $\partial^2 E_{-1}(z)/\partial z^2 = 0$ and $\partial^2 E_0(z)/\partial z^2 = 0$), yields

$$\begin{aligned} & \left[(k_x^2 + \gamma_{z,0}^2) E_0(z) - 2i\gamma_{z,0} \frac{\partial E_0(z)}{\partial z} \right] e^{-i(k_x x + \gamma_{z,0} z - \omega_0 t)} \\ &+ \left[(k_x^2 + \gamma_{z,-1}^2) E_{-1}(z) - 2i\gamma_{z,-1} \frac{\partial E_{-1}(z)}{\partial z} \right] e^{-i(k_x x + \gamma_{z,-1} z - \omega_{-1} t)} \\ &= \frac{1}{c^2} \left(\left[\omega_0^2 \epsilon_{\text{av}} + \frac{\epsilon_{\text{m}}}{2} (\omega_0 - \omega_{\text{m}})^2 e^{i(\beta_{\text{m}} z - \omega_{\text{m}} t)} + \frac{\epsilon_{\text{m}}}{2} (\omega_0 + \omega_{\text{m}})^2 e^{-i(\beta_{\text{m}} z - \omega_{\text{m}} t)} \right] E_0(z) e^{-i(k_x x + \gamma_{z,0} z - \omega_0 t)} \right. \\ & \quad \left. + \left[\omega_{-1}^2 \epsilon_{\text{av}} + \frac{\epsilon_{\text{m}}}{2} (\omega_0 - 2\omega_{\text{m}})^2 e^{i(\beta_{\text{m}} z - \omega_{\text{m}} t)} + \frac{\epsilon_{\text{m}}}{2} \omega_0^2 e^{-i(\beta_{\text{m}} z - \omega_{\text{m}} t)} \right] E_{-1}(z) e^{-i(k_x x + \gamma_{z,-1} z - \omega_{-1} t)} \right). \end{aligned} \quad (\text{S5})$$

We then multiply both sides of Eq. (S5) with $e^{i(k_x x + \gamma_{z,0} z - \omega_0 t)}$, which gives

$$\begin{aligned} & \left[(k_x^2 + \gamma_{z,0}^2) E_0(z) - 2i\gamma_{z,0} \frac{\partial E_0(z)}{\partial z} \right] \\ &+ \left[(k_x^2 + \gamma_{z,-1}^2) E_{-1}(z) - 2i\gamma_{z,-1} \frac{\partial E_{-1}(z)}{\partial z} \right] e^{i(\beta_{\text{m}} z - \omega_{\text{m}} t)} \\ &= \frac{1}{c^2} \left(\left[\omega_0^2 \epsilon_{\text{av}} + \frac{\epsilon_{\text{m}}}{2} (\omega_0 - \omega_{\text{m}})^2 e^{i(\beta_{\text{m}} z - \omega_{\text{m}} t)} + \frac{\epsilon_{\text{m}}}{2} (\omega_0 + \omega_{\text{m}})^2 e^{-i(\beta_{\text{m}} z - \omega_{\text{m}} t)} \right] E_0(z) \right. \\ & \quad \left. + \left[\omega_{-1}^2 \epsilon_{\text{av}} + \frac{\epsilon_{\text{m}}}{2} (\omega_0 - 2\omega_{\text{m}})^2 e^{i(\beta_{\text{m}} z - \omega_{\text{m}} t)} + \frac{\epsilon_{\text{m}}}{2} \omega_0^2 e^{-i(\beta_{\text{m}} z - \omega_{\text{m}} t)} \right] E_{-1}(z) e^{i(\beta_{\text{m}} z - \omega_{\text{m}} t)} \right), \end{aligned} \quad (\text{S6})$$

and next, applying $\int_0^{\frac{2\pi}{\omega_{\text{m}}}} dt$ to both sides of (S6) yields

$$\frac{dE_0(z)}{dz} = i \frac{\epsilon_{\text{m}} k_0^2}{4\gamma_{z,0}} E_{-1}(z). \quad (\text{S7})$$

Following the same procedure, we next multiply both sides of (S6) with $e^{-i(\beta_{\text{m}} z - \omega_{\text{m}} t)}$, and applying $\int_0^{\frac{2\pi}{\omega_{\text{m}}}} dt$ in both sides of the resultant, which reduces to

$$\left[(k_x^2 + \gamma_{z,-1}^2) E_{-1}(z) - 2i\gamma_{z,-1} \frac{dE_{-1}(z)}{dz} \right] = \frac{\omega_{-1}^2}{c^2} \left(\frac{\epsilon_{\text{m}}}{2} E_0(z) + \epsilon_{\text{av}} E_{-1}(z) \right), \quad (\text{S8})$$

$$\frac{dE_{-1}(z)}{dz} = i \frac{\epsilon_m k_{-1}^2}{4\gamma_{z,-1}} E_0(z), \quad (\text{S9})$$

where $k_{-1} = \omega_{-1}/c^2$. Solving the coupled equations (S7) and (S9) together, we achieve the field coefficients $E_0(z)$ and $E_{-1}(z)$ as given in Eqs.(17) and (18) for the reception state and in Eqs.(23) and (24) for the transmission state.
